Alloy broadening and bowing of energy gaps of $In_{1-x}Ga_xAs_yP_{1-y}$/InP derived from low-temperature electroreflectance

C. Reh and G. Weiser
Department of Physics and Material Sciences Center, Philipps-University, Marburg, 35032 Marburg, Germany
(Received 15 August 2001; published 28 December 2001)

Spectra of single crystals over the full composition range have been measured up to 5.5 eV and are compared with the theory of van Hove singularities in an electric field to achieve the accuracy needed for the evaluation of compositional trends. For the fundamental gap the high-field limit applies and moderate fields influence the spectral line shape at higher energy despite increasing lifetime broadening. Alloy broadening is smaller for gaps at Γ than for noncenter singularities. The compositional shift of nine gaps shows large variation of bowing which is largest for the saddle point E_1 at L. The deviations from the virtual crystal model are attributed to intraband scattering on the random disorder potential proposed by Van Vechten and Bergstresser but details of the density of states distribution and of intraband scattering matrix elements are important to understand the variations. Gaps at Γ are most sensitive to fluctuation on the cation sublattice. Compositional fluctuation of the anions increases the spin-orbit splitting in the valence band without a significant difference for Δ_0 and Δ_1.

DOI: 10.1103/PhysRevB.65.035321 PACS number(s): 78.20.Jq, 71.20.Nr, 78.66.Fd

I. INTRODUCTION

The technological interest in the quaternary semiconductor $In_{1-x}Ga_xAs_yP_{1-y}$ led to considerable effort and success in growing alloy crystals of high quality. Lattice match to InP substrates is possible by keeping the ratio $y/x=2.14$ and enables epitaxial growth of strain-free bulk samples from InP to the ternary alloy $In_{0.53}Ga_{0.47}As$. These alloys provide an excellent system to study the influence of disorder on the band structure of semiconductors. The disadvantage of having disorder on both sites of the zinc-blende lattice is compensated by the vanishing of intrinsic effects resulting from the changing lattice constant in ternary alloys. Deviations from the virtual crystal approximation (VCA), the linear interpolation of lattice potential and gaps, thus result from the nonperiodic potential due to compositional fluctuation. Ternary alloys show a quadratic bowing $C(y)$ of the gap below the values of a linear interpolation which defines a bowing potential $D(y)$ arising from the random distribution of ions on one sublattice:

$$E_g(y)=A+By+Cy^2=\mathcal{A}+(\mathcal{B}-\mathcal{A})y-Dy(y-1). \quad (1)$$

$\mathcal{A}$ and $\mathcal{B}$ are the gaps of the binary compounds ($y=0$) and ($y=1$), respectively. Van Vechten and Bergstresser found that intrinsic bowing in a virtual crystal is much smaller than bowing due to the disorder potential which they modeled from the different electronegativity of ions.[1] Pearsall extended this approach to lattice-matched (InGa)(AsP)/InP and derived a value $C=0.15$ eV for the fundamental gap.[2] This bowing parameter was in fair agreement with bowing derived from photoluminescence[3] and electroreflectance spectra.[4–6] Van Vechten and Bergstresser conjectured further a short-range disorder potential since the atomic fluctuations in neighboring cells are uncorrelated and predicted that all gaps between a pair of valence and conduction bands have the same bowing regardless of their position in the Brillouin zone. Since the few and widely scattering electroreflectance data seemed compatible with this conjecture, Pearsall proposed a common bowing parameter $C(y)$ for all gaps of (InGa)(AsP). Estimates from second-order perturbation theory confirm a reduction of the gap by disorder, but predicting a decreasing bowing for higher-lying energy gaps they contradict a universal bowing of energy gaps.[7] Similar uncertainty exists for the influence of disorder on spin-orbit splitting.

Previous electroreflectance spectra which provided data for high-energy gaps have been measured at room temperature by modulating the field on an electrolyte-semiconductor interface, which results in a spectral linewidth comparable or larger than the bowing parameter. More accurate values of the gaps were derived from approximate line shape fits which compare the relative size of peaks in a spectrum as proposed for the low-field limit where the line shape is determined by lifetime broadening.[8] Since this procedure may be misleading if the response of different gaps overlap, Kelso *et al.* derrived the gaps from ellipsometric measurements of the dielectric function $\varepsilon(\omega)$.[9] An elaborate line shape analysis employed the equivalence of the third derivative of $\varepsilon(\omega)$ and the field-modulated spectra which again is valid for the low-field case.[10] For the gap E_1 at L, which they attributed to a saddle-point singularity M_1, they found significantly larger bowing than electroreflectance studies.

Accurate values of the compositional variation of energy gaps require spectra of narrower spectral linewidth. We performed therefore low-temperature electroreflectance studies, and by comparing the spectra with the theory of field-induced changes of van Hove singularities in the presence of lifetime broadening, we avoided the presumption of the low-field limit.[11,12] Although the low-field limit is supported by the third derivative line shape of the electroreflectance spectrum of Ge in the vicinity of the E_1 gap,[13] it is not applicable to electroabsorption spectra of (InGa)(AsP) alloys at the fundamental gap which show numerous Franz-Keldysh oscillations in rather small fields in perfect agreement with the

theory of the Franz-Keldysh effect for the high-field limit.[14,15] The range of oscillations increases linearly with field and corresponds to the energy optically excited electron hole pairs acquire in an electric field before scattering destroys the coherent motion. The mean free path is independent of the field and varies between 60 nm for quaternary and 160 nm for ternary alloys.[16] Although scattering rates increase with excess energy, it was uncertain that large fields anticipated on the surface of a sample comply with the low-field limit of electroreflectance spectra.

II. EXPERIMENTAL DETAILS

A series of 600-nm-thick samples has been deposited by low-pressure metal-organic chemical vapor deposition (MOCVD) on (001)-oriented *n*-doped InP substrates which served as a grounded electrode. InP cap layers were etched off, and a semitransparent 5-nm thin Pt contact was evaporated as the top electrode. The contact defined a $4\times3\ \mathrm{mm}^2$ large area which was investigated by high-resolution x-ray spectra to determine the residual lattice mismatch and to correct for strain-induced shifts of the fundamental gap. The lattice mismatch $\Delta a/a$ of most samples was below 10^{-3}, which kept such corrections negligibly small. Comparative studies of samples grown by liquid phase epitaxy (LPE) show the same quality of spectra. The samples were mounted to the tip of a He flow cryostat and cooled to 20 K. Electroreflectance spectra were measured with a bandpass less than 1 meV in the visible, which increased to 8 meV at the shortest wavelength. This wider bandpass combined with long integration times was needed to keep the noise level at 10^{-6}, at least one order of magnitude below the weak signals of some alloys near 5 eV. A cooled Ge detector for the IR and multipliers at higher energy measured dc and ac components of the reflected light. A square pulse modulation of 1 kHz frequency was used, and particular attention was paid to the phase of the signal which was checked by comparison with the field-induced absorption below the absorption edge. A positive signal $\Delta R/R$ corresponds to an increase of the reflectivity with increasing field.

The comparison to theoretical line shape requires knowledge of the dielectric function $\varepsilon(\omega)$ which was derived by Kramers-Kronig transformation of reflectance spectra at 80 K and keeping the sample surrounded by walls cooled to liquid nitrogen. The higher temperature was chosen to avoid surface contamination by condensation of residual air in the vacuum chamber. Reflectance spectra were measured between 0.75 and 10 eV using a 0.5-m vacuum monochromator and LiF windows. The experimental reflectivity R was extrapolated beyond $E_{\max}=10\ \mathrm{eV}$ using a power-law decrease $R(E)/R(E_{\max})=(E_{\max}/E)^p$, with p chosen to reproduce the position of the absorption edge.

III. EXPERIMENTAL RESULTS

A. Survey of the optical spectra

The reflectance spectra in Fig. 1 have the characteristic shape of cubic semiconductors with maxima related to regions of large joint density of states and arising from transitions from the top valence band. Spin-orbit coupling splits the first maximum E_1, attributed to the gap at L, into a doublet. The second maximum near 5 eV has contributions from several gaps like E_2 on the [100] axis or in X and from the second gap E_0' at Γ. The smallest gap to the first conduction band E_0 at Γ is not resolved due to the low density of states. Although the spectra of alloys are broadened, they maintain this shape of cubic single crystals, which confirms that alloy scattering is too small to destroy the long-range order.

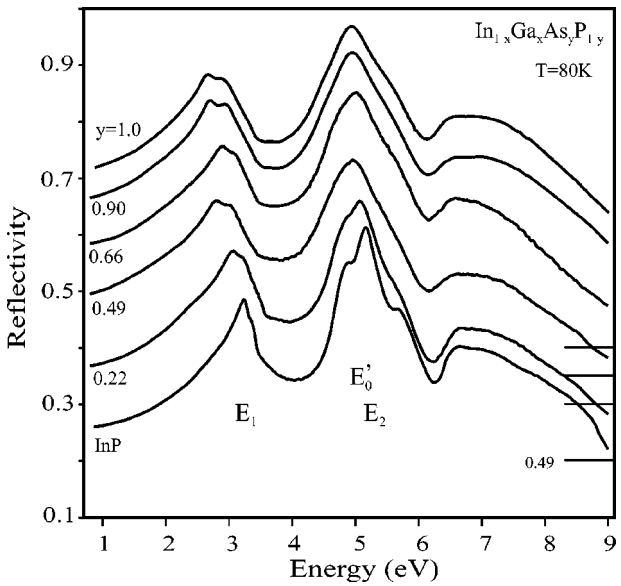

FIG. 1. Reflectance spectra of $In_{1-x}Ga_xAs_yP_{1-y}$/InP. The ordinate corresponds to InP: the baseline of the alloys is shown on the right.

Spectra $\varepsilon_1+i\varepsilon_2$ of the real and imaginary parts of the dielectric constant ε are very similar to those obtained by ellipsometry at room temperature below 6 eV.[9] Figure 2 presents spectra of the absorption constant α which reveal the small penetration depth of light $(1/\alpha)$, 12 nm near E_1 and 7

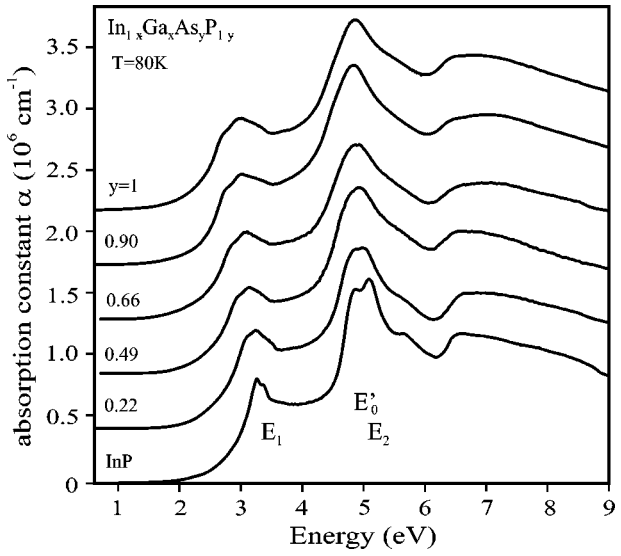

FIG. 2. Absorption spectra of $In_{1-x}Ga_xAs_yP_{1-y}$/InP.

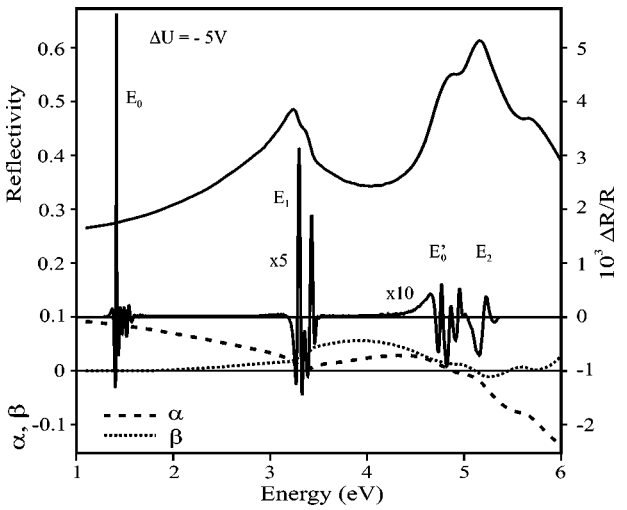

FIG. 3. Comparison of reflectance and electroreflectance spectra of InP. Parts of the electroreflectance spectra has been enlarged with respect to scale. α and β are the Seraphin coefficients.

nm at E_2, compared to 1 μm near the fundamental gap. Electroreflectance spectra of high-lying gaps therefore depend on modulation of the field near the Pt interface by the external voltage, while the spectrum at E_0 depends on the field in the sample. The absorption peak of the spin doublet E_1 shows increasing height of the upper peak, which has also been noticed in ellipsometric measurements. Such a change suggests some redistribution of oscillator strength, but in absorption spectra they are enhanced by the decrease of the refractive index above the resonance and by the increased splitting at larger As content. Changes in ε_2 spectra are smaller and could not be evaluated because of the large spectral linewidth.

The improvement in spectral linewidth by electroreflectance spectroscopy is evident from a direct comparison of spectra of InP in Fig. 3. The largest signal is observed at the fundamental gap E_0, the spin doublet E_1 is clearly resolved, and the spectrum near 5 eV confirms the complex structure of the second reflectance peak near 5 eV. The leading signals in this range are distinctly below the reflectance shoulder at 4.85 eV and thus should correspond to gaps of low density of states. The general features agree quite well with the earliest electroreflectance spectrum of InP obtained on an electrolyte interface at room temperature.[17]

The electroreflectance spectrum contains contributions from changes of the real and imaginary parts of the dielectric constant:

$$\frac{\Delta R}{R}=\alpha(\varepsilon_1,\varepsilon_2)\Delta\varepsilon_1+\beta(\varepsilon_1,\varepsilon_2)\Delta\varepsilon_2. \tag{2}$$

The Seraphin coefficients[18] α and β are derived by Kramers-Kronig analysis of the reflectivity and are shown in the lower part of Fig. 3. They are much smaller than 1 and reveal some loss of sensitivity with respect to electroabsorption spectra, which, however, are restricted to the absorption edge. Electroreflectance spectra of E_0 are determined exclusively by changes of $\Delta\varepsilon_1$, while at higher energy the line shape is

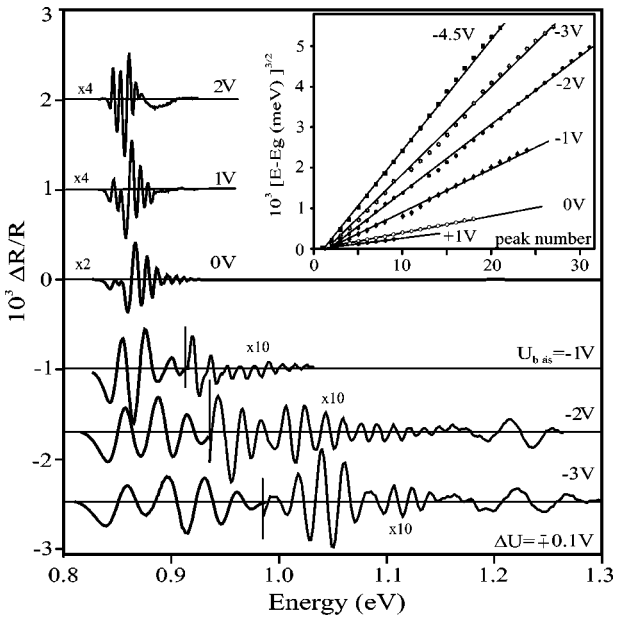

FIG. 4. Electroreflectance spectra near the fundamental gap of a quaternary alloy ($y=0.9$) measured with small modulation voltage ΔU for different bias voltage. Part of the spectra are enlarged with respect to scale. The inset shows the relationship of position and number of extrema of Franz-Keldysh oscillations.

complicated due to contributions of $\Delta\varepsilon_1$ and $\Delta\varepsilon_2$, which makes approximate line shape fits unreliable. We found the Seraphin coefficients to be fairly stable with respect to moderate variation of absolute reflectivity and to the extrapolations to high energy.

B. Spectra at the fundamental gap E_0

The sensitivity of the fundamental gap to electric fields enables a derivative type of electroreflectance where the field in the sample is defined by a dc bias and varied by a small modulation voltage.[15] This modulation technique yields more detailed spectra as shown in Fig. 4 by a series of spectra of a quaternary sample. Under reverse bias numerous Franz-Keldysh oscillations develop which broaden with increasing field. This common line shape results from renormalization of the energy of free electrons to an electro-optic energy $\hbar\theta$, which accounts for the changing momentum and stretches the spectra proportional to $F^{2/3}$. The shift of a particular peak E_n away from the band gap E_g follows a useful relationship of peak energy, peak number n, and field F:

$$(E_n-E_g)^{3/2}=\frac{3eh}{8\sqrt{2}}\frac{F}{\sqrt{m^*}}n. \tag{3}$$

This relation identifies the high-field case and applies here as shown by the inset in Fig. 4. From the reduced mass $m^*=0.04m_0$ of the dominant heavy-hole transitions, we find an increase of the field from 4.3 kV/cm at 1 V forward bias to 38 kV/cm at -4.5 V reverse bias. The beat in the spectra results from superposition with the weaker series of light-hole transitions of smaller reduced mass and from switching between two fields by a small modulation voltage. Similar

beats have been observed in photomodulation spectra of GaAs (Refs. 19 and 20) and have been analyzed as Franz-Keldysh oscillations.[21] The spectra demonstrate the high-field case even for fields as low as 4 kV/cm. The range where oscillations are observed increases linearly with field and corresponds to the energy which an electron-hole pair acquires in the field before scattering destroys its coherence. The coherence length is 125 nm in this quaternary sample.[16] Another series of oscillations is observed above 1.2 eV, which starts at the gap $E_0+\Delta_0$ of the split-off split-off valence band at Γ.

For zero ($F=5.3$ kV/cm) and forward bias some fine structure of the first peaks develops which is attributed to bound states of light- and heavy-hole excitons. The presence of two excitons in small fields is consistent with the relatively large tensile strain in this sample ($\Delta a/a=-3.2\times10^{-3}$), which splits the valence bands at Γ by 11 meV. The field mixes unbound and bound exciton states, which at low fields remain visible as resonant states, but are no longer resolved at 15 kV/cm (-1 V bias).[15,22,23] The first zero of electroabsorption spectra which are equivalent to $\Delta\varepsilon_2$ moves very little with field and defines the gap as origin of Franz-Keldysh oscillations. This gap is not the single-particle gap of the band structure and lies slightly below the heavy-hole exciton.

The shift of the numerous oscillations according to Eq. (3) indicates a fairly homogeneous field in the sample which increases almost linearly with bias. Therefore, although we are using a Pt contact, the experimental situation differs from Schottky barrier electroreflectance measurements on thick single crystals where the field varies with the square root of the applied voltage.[24] The field in our samples results not from space charge in the sample, but from exchange of charge between contacts of different Fermi levels as in a pin diode. Small inhomogeneity of the field does not lead to destructive interference of the Franz-Keldysh effect in different regions[14] which favors the use of thin samples in photo- and electroreflectance spectroscopy where residual space charge does not add up to a large field.

The compositional shift of the fundamental gap is shown in Fig. 5. The spectra were obtained by switching from zero to a large reverse voltage of 5 V, the same condition which is used for the high-energy gaps. A smaller voltage has been used for InP to resolve the signal of the split-off band above 1.5 eV, which otherwise would be obscured by oscillations from the fundamental gap (see Fig. 3). The spectra show some enhancement of the leading peaks which is due to the excitonic contribution at low field. The significant broadening of the spectra of all alloys cannot be attributed to the high field and agrees with trends of the low-field exciton linewidth and the coherence length of continuum states in electroabsorption measurements.[14,16] Line shape analysis shows linewidth broadening $\Gamma<5$ meV, which is much smaller than the electro-optical energy $\hbar\theta\approx25$ meV. The signal amplitude depends also on the field modulation by the external voltage, which varies for different sample despite their same thickness since part of the external voltage is screened by charge on the interfaces to substrate and Pt contact.[15]

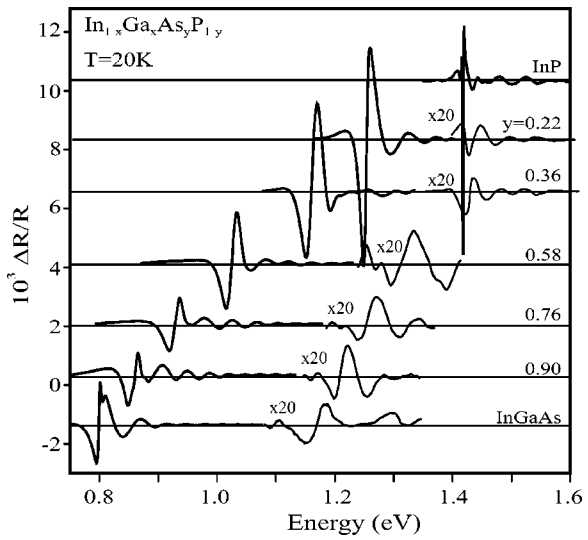

FIG. 5. Variation with composition of the electroreflectance spectra of E_0 and $E_0+\Delta_0$ transitions. $\Delta U=-5$ V and zero bias. Part of the spectra have been enlarged with respect to scale.

C. Energy gap E_1 at L

Electroreflectance spectra of the next gap E_1 (Fig. 6) have much broader linewidth than spectra of E_0 due to a rapid loss of coherence at high energy. The narrower linewidth in the case of InP indicates that compositional fluctuations broaden the band gap singularity with surprisingly little variation among the alloys. Since the Seraphin coefficient β is larger than α in this spectral range, the line shape of the electroreflectance spectrum is close to that of $\Delta\varepsilon_2$. All spectra begin with a negative peak similar to that as observed in GaAs (Refs. 24 and 25) and Ge (Ref. 13). This line shape corresponds to a saddle-point singularity of type M_1 and a transverse field, i.e., the field in the direction of the positive re-

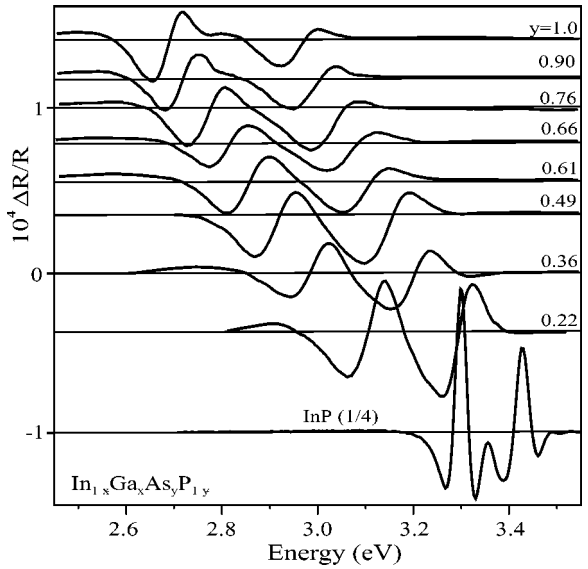

FIG. 6. Variation with composition of the electroreflectance spectra of E_1 and $E_1+\Delta_1$ transitions. The spectrum of InP is reduced in size as indicated. $\Delta U=-5$ V and zero bias.

duced mass. Our line shape analysis follows the scheme given by Aspnes[11,12] which is based on the difference of Airy functions Ai(z), eigenstates in a constant field, and the plane-wave states in a constant potential. The dielectric function $\varepsilon(E)$ near a van Hove singularity in an electric field is described by a combination of an Airy function Ai(z) and its derivative Ai$'(z)$. The complex argument z represents the energy with respect to E_g of the singularity and the lifetime broadening Γ of an electron-hole pair. Both are normalized to the electro-optic energy $\hbar\theta$, which accounts for the spatial variation of the potential due to the field F:

$$z=\xi+i\,\eta=\frac{E_g-E}{\hbar\theta}+\frac{i\,\Gamma}{\hbar\theta},\quad (\hbar\theta)^3=\frac{(eF\hbar)^2}{2m^*}. \tag{4}$$

The imaginary part which corresponds to Lorentzian broadening leads for the low-field case ($\hbar\theta \ll \Gamma$) to a strong reduction of the signal and to a line shape independent of the field. Nearly parallel conduction and valence bands along [111] with a slightly larger dispersion of the valence band results in a negative reduced longitudinal mass m_L and a saddle-point singularity of type M_1 at L since the transverse reduced mass m_T remains positive.[26] The anisotropic mass modifies the electro-optic energy, which is the sum of projections of the field F onto the axes of the mass tensor, and yields for $F\|[001]$

$$(\hbar\theta)^3=\frac{(e\hbar)^2}{2}\left(\frac{2}{3}\frac{F^2}{m_T}+\frac{1}{3}\frac{F^2}{m_L}\right). \tag{5}$$

Positive and negative, respectively, signs distinguish the transverse and longitudinal cases of the saddle-point spectrum. Since the longitudinal mass is large, $\hbar\theta$ is given by the transverse mass.

Equation (6) describes $\Delta\varepsilon$ near the M_0 singularity of a gap like E_0 as a difference to the density of states in the field-free case which depends on the square root of energy. The prefactor accounts for the optical matrix elements and $w=z\exp(-i2\pi/3)$:

$$\Delta\varepsilon_1(\xi,\eta)=B\frac{\sqrt{\hbar\theta}}{\omega^2}\left\{2\pi\,\mathrm{Im}\left[\exp\left(-i\frac{\pi}{3}\right)\mathrm{Ai}'(z)\mathrm{Ai}'(w)+w\,\mathrm{Ai}(z)\mathrm{Ai}(w)\right]+\sqrt{\frac{|z|+\xi}{2}}\right\},$$

$$\Delta\varepsilon_2(\xi,\eta)=B\frac{\sqrt{\hbar\theta}}{\omega^2}\left\{2\pi\,\mathrm{Re}\left[\exp\left(-i\frac{\pi}{3}\right)\mathrm{Ai}'(z)\mathrm{Ai}'(w)+w\,\mathrm{Ai}(z)\mathrm{Ai}(w)\right]-\sqrt{\frac{|z|-\xi}{2}}\right\}. \tag{6}$$

The expressions for the saddle point emphasize the relationships between van Hove singularities:

$$\Delta\varepsilon_1(M_0)=\Delta\varepsilon_2(M_{1T})=\Delta\varepsilon_1(M_{1L}),$$

$$\Delta\varepsilon_2(M_0)=-\Delta\varepsilon_1(M_{1T})=-\Delta\varepsilon_2(M_{1L}). \tag{7}$$

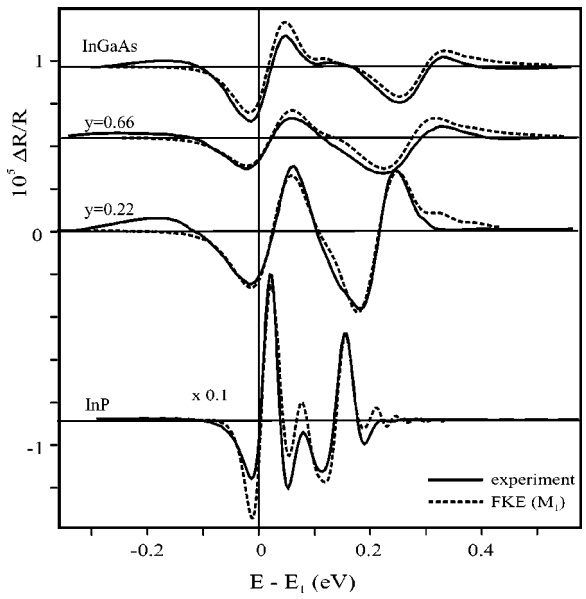

FIG. 7. Line shape analysis of electroreflectance spectra of the spin doublet at E_1.

For the longitudinal case ξ has to be replaced by $-\xi$ since the critical point energy is the upper border of the continuum along the field. Real and imaginary parts obey Kramers-Kronig relations and are oscillating functions of similar shape with their difference further obscured by lifetime broadening. A clear distinction of spectra of a transverse saddle point and a band gap is the opposite sign of their $\Delta\varepsilon_2$ spectra.

Figure 7 shows the good agreement of experimental spectra of $\Delta R/R$ with those calculated for two transverse saddle points M_1 at E_1 and $E_1+\Delta_1$. The reference energy is the gap E_1 slightly above the first negative peak of the experimental spectrum. Parameters of the fit are the transition energy, broadening, and amplitude at each gap while the electro-optic energy $\hbar\theta$ was assumed to be the same. It is not possible to match the width of the narrow spectrum of InP by adjusting the broadening parameter Γ alone, but only by an appropriate choice of the field. We find a rather small value of $\hbar\theta=27$ meV, equivalent to $F=50$ kV/cm for a mass $m^*=0.05m_0$. This mass is similar to the mass in GaAs (Ref. 24) and Ge (Ref. 27) as derived from a small number of Franz-Keldysh oscillations in a much higher field. The field thus is comparable to that inside the sample, again a distinct difference to Schottky barrier spectra. The ratio 5:4 of the amplitudes is consistent with the absorption spectrum and the higher transition shows larger broadening, $\Gamma=23$ meV compared to 18 meV for the lower transition. Since broadening parameter and $\hbar\theta$ are similar, the low-field case does not apply. We observe indeed some change of line shape if low-field modulation is employed, but no Franz-Keldysh oscillations which in the calculated spectrum extend 200 meV beyond the gap. The range of Franz-Keldysh oscillations is limited by the spatial coherence of the optically excited state which cannot exceed the penetration depths of light. The coherence thus should be about 15 nm, one order of magnitude smaller than the coherence length at the absorption

edge.[14,28] For fields applicable to our samples Franz-Keldysh oscillations of E_1 could extend at most 100 meV beyond the gap and may also be smeared out by the larger inhomogeneity of the field near the surface.

The range of parameters for a good fit of the InP spectrum is fairly limited, but increases for the broader spectra of the alloys since the field, amplitude, and broadening affect the line shape simultaneously. Nevertheless, a good match is only achieved with a contribution of the field to the spectral width. The spectrum of the ternary compound is reproduced by $\hbar\theta = 35$ meV, the same amplitude, and $\Gamma = 55$ and 72 meV, respectively, for the lower and upper transitions. These values can be varied by 10%, since changes due to the variation of one parameter can be compensated by an appropriate choice of the others. For the quaternary alloys fit parameters are $\hbar\theta = 41$ and 43 meV and $\Gamma = 55$ and 70 meV, for $y = 0.22$ and 0.66, respectively. These numbers again are consistent with trends in the excitonic linewidth and the coherence length at the fundamental gap of the alloys. The most stable parameter is the transition energy, which is insensitive to a moderate variation of the parameters.

The good fit to the spectra may be surprising since it employs Seraphin coefficients which are derived from Kramers-Kronig analysis of the reflectivity of a free surface while electroreflectance spectra were measured through a thin Pt film. This film causes an additional phase shift of the reflected light, which alters the ratio of the Seraphin coefficients. These changes evidently are small in the range of interest in accordance with model calculations for a thin Ni film on Ge.[29] InP, which is most sensitive because of the narrow linewidth, shows indeed some deficit in the fit to the size of positive and negative peaks. After a small increase of α by 0.02, which exceeds the variation observed in Kramers-Kronig transformations, the difference in the negative peaks of experimental and calculated spectra disappears due to the larger contribution of $\Delta\varepsilon_1$ and this contribution shifts the gap by 3 meV to lower energy.

D. High-energy region

The next gap E_0' is at the center of the Brillouin zone with transitions from the top of the valence band Γ_8^v to the Γ_7^c and Γ_8^c conduction bands which split by Δ_0' due to spin-orbit coupling.[26] A saddle-point singularity $\delta(M_1)$ is predicted at slightly higher energy and 20% off the zone center on the [100] where the crystal field removes the degeneracy on the crossover of two conduction bands in a diamond lattice (Ge). Most of the absorption near 5 eV is attributed to the large joint density of states of the uppermost valence and the lowest conduction band along [100] with the singularity E_2 at X on the edge of the Brillouin zone. The $\Delta\varepsilon_2$ spectrum of InP (Fig. 8) displays the anticipated complex line shape in close resemblance to the low-temperature spectrum of GaAs.[24] Four transitions are resolved in the range of E_0' followed by a broader signal near 5.1 eV, which tentatively is attributed to E_2. Only the lowest two are well resolved in spectra of the alloys, while the others become weak structures and kinks on the strongly broadening response of E_2.

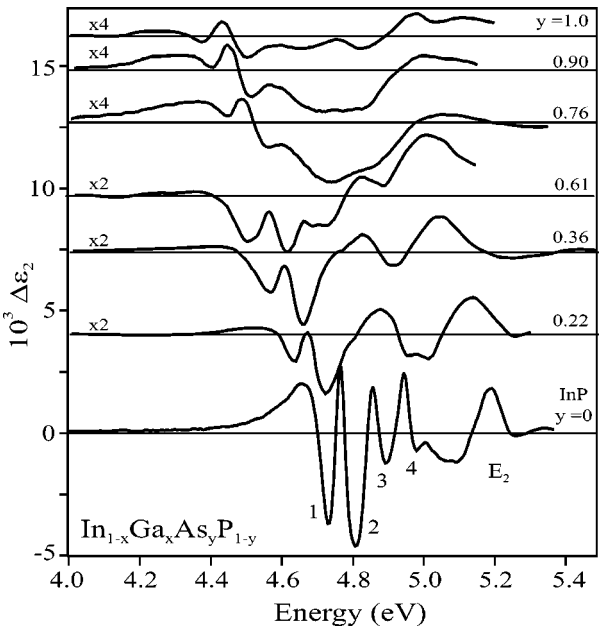

FIG. 8. Spectra $\Delta\varepsilon_2$ in the vicinity of E_0' and E_2 transitions. Spectra of the alloys have been enlarged as indicated. $\Delta U = -5$ V and zero bias.

The line shape analysis of the spectrum of InP is presented in Fig. 9. Two features E_0' and $E_0' + \Delta_0'$ are attributed to the zone center gaps, which are M_0 singularities. The situation is more complicated for the singularity δ near (0.2,0,0). Splitting of degenerate conduction bands results in opposite curvature of the bands, resulting in a saddle point M_1 for the lower and an M_0 singularity for the upper band. In contrast to the saddle point E_1 at L the projection of the field F onto the mass tensor axes is different for the six equivalent $\delta(M_1)$ singularities. Two correspond to the longitudinal and four to the transverse case which have a dis-

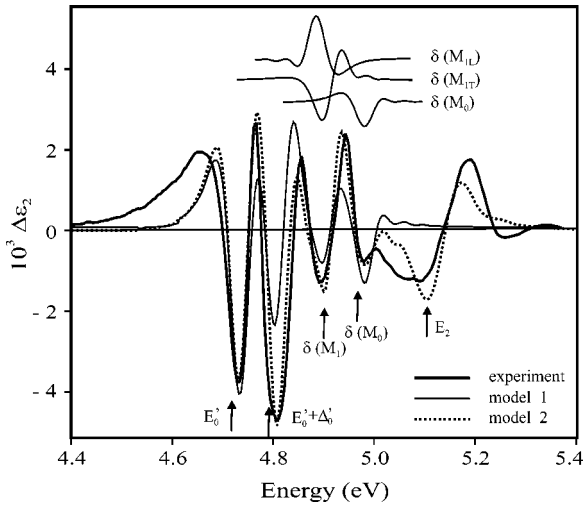

FIG. 9. Line shape analysis of the $\Delta\varepsilon_2$ spectrum of InP in the range of E_0' and E_2 transitions. The assignment corresponds to model 2. Model 1 attributes the second transition to the saddle point δ. The top shows the different line shape of the response of the δ singularities.

TABLE I. Fit parameter to the electroabsorption spectrum of InP in the range of the E_0' transition (Fig. 9) for two different assignments of the saddle point singularity $\delta(M_1)$. $\hbar\theta = 26$ meV corresponding to a field of 50 kV/cm for $m^* = 0.05 m_0$.

	Model 1				Model 2			
Gap	E_0'	$\delta(M_1)$	$E_0'+\Delta_0'$	$\delta(M_0)$	E_0'	$E_0'+\Delta_0'$	$\delta(M_1)$	$\delta(M_0)$
$\hbar\omega$ (eV)	4.716	4.800	4.880	4.965	4.716	4.792	4.901	4.965
Type	M_0	$M_{1T}M_{1L}$	M_0	M_0	M_0	M_0	$M_{1T}M_{1L}$	M_0
Amplitude	20	45 50	40	20	42	45	33 6	16
Γ (meV)	33	40	33	35	33	33	33	35

tinctly different line shape as shown on top of Fig. 9. The larger number of transverse saddle points favors that line shape since the dominance of the longitudinal line shape requires a very small longitudinal mass along [100]. The total line shape depends on the sequence of singularities. Model 1 uses the sequence E_0', $\delta(M_1)$, $E_0'+\Delta_0'$, and $\delta'(M_0)$, which has been proposed for GaAs, while model 2 reverses the order of $E_0'+\Delta_0'$ and $\delta(M_1)$ using, except for some change of the amplitude, the same parameters for the other transitions (Table I). The electro-optic energy was 26 meV, again very similar to the spectra of the other regions at 5 V. Model 2 reproduces the line shape in the center of the quadruplet much better with a small and insignificant contribution of the longitudinal saddle point. We propose therefore the level ordering of model 2, which is indicated in the figure. This assignment is different from that conjectured from line shape analysis of ellipsometric spectra,[9] but agrees with the assignment by Laufer *et al.*[5] The δ singularities result from the loss of inversion symmetry in the zinc-blende lattice. We expect therefore a particular sensitivity to compositional fluctuations, which is confirmed by their rapid broadening in all alloys while the leading features 1 and 2 remain well resolved (Fig. 8). A fit of these two features in the ternary compound yields satisfactory agreement for $\Gamma = 70$ meV and $\hbar\theta = 42$ meV, similar to the parameters which fit the spectrum of E_1.

The last feature in Fig. 9 is attributed to E_2 and shows a rather large linewidth even in InP. We show a calculated spectrum for a M_1 singularity at 5.105 eV, 80 meV linewidth, and $\hbar\theta = 36$ meV with contributions of transverse and longitudinal line shapes in the ratio 2:1. Except for a longitudinal M_2 singularity, no other type of singularity provides a similar good approximation. The strong alloy broadening and the poor fit indicates unresolved contributions from several singularities, for instance, due to small spin-orbit splitting of the valence band along [100].

IV. DISCUSSION

A. Compositional shift of energy gaps

The low-temperature spectra resolve nine critical points and provide data to follow compositional trends over a wide range of energy. We used different definitions of the gap energies shown in Fig. 10 to obtain the compositional shifts most accurately. For the spin-doublet E_0 electroabsorption spectra give the best accuracy since they correspond to $\Delta\varepsilon_2$ without requiring Kramers-Kronig transformation of experimental spectra. The gap is attributed to the origin of Franz-Keldysh oscillations which in the presence of fields and disorder is a better definition of the onset of a band continuum since it includes the Coulomb coupling of coherently excited electron-hole pairs. The weak Coulomb potential creates states below the single-electron gap, but the boundary between bound and unbounded pair states is indistinguishable even for vanishing field.[30] For the spin-doublet E_1 the gap is derived from the line shape analysis of the electroreflectance spectra. Except for InP such an analysis was not meaningful for the broad features above 4 eV. We used therefore the first negative peaks of $\Delta\varepsilon_2$ spectra which are best identified. This procedure gives slightly too large gaps, but has a small effect on their shift with composition because of the similar linewidth of all alloy spectra. All gaps have negative bowing

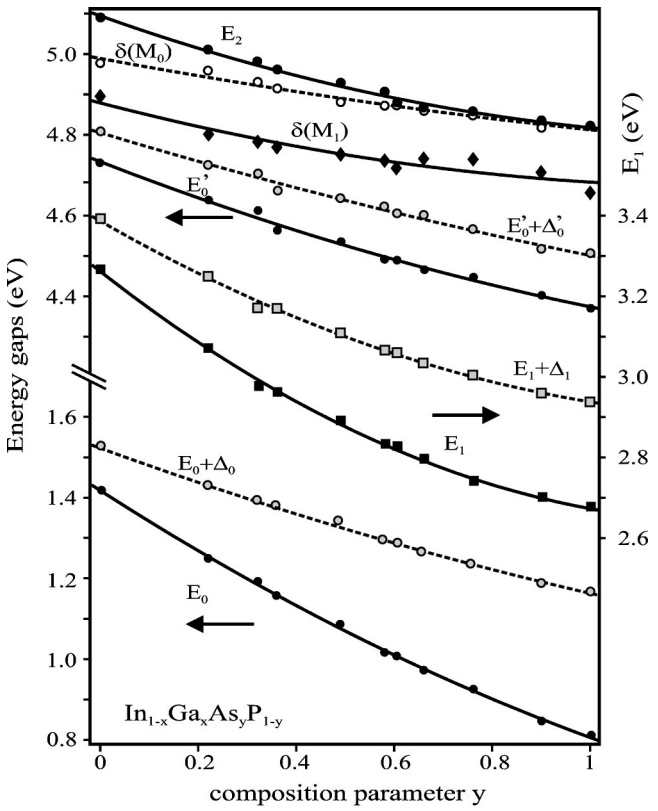

FIG. 10. Compositional variation of energy gaps of $In_{1-x}Ga_xAs_yP_{1-y}$. The curves are fits to Eq. (1).

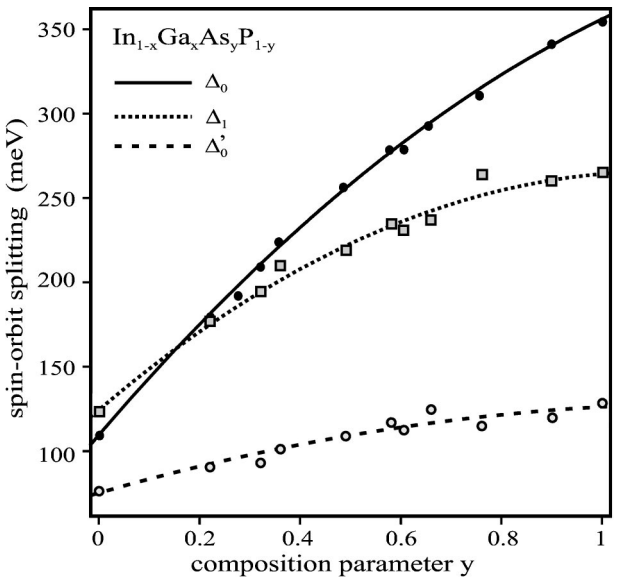

FIG. 11. Compositional variation of spin-orbit splitting of valence and conduction bands. The curves are fits to Eq. (1).

below the value of a linear shift between InP and the ternary compound. Bowing of the upper gap of spin doublets is smaller, which reflects the positive bowing of spin-orbit splitting shown in Fig. 11.

Table II summarizes the result of least-squares fits to the compositional shift of energy gaps and compares the bowing parameter C with the literature data [Eq. (1)]. The variance of gap energies is small because of the improved resolution of low-temperature spectra, but adds up if the deviation from a linear shift, the bowing parameter C, is extracted. Nevertheless, in most cases the variance of C remains below 25 meV, much smaller than its value. The variation of the two gaps attributed to δ is less accurate due to the large linewidth and weakness of their response in alloy spectra. The literature data scatter strongly and are often outside the range of our data. For the spin doublet E_1 we find good agreement with the result of the elaborate line shape analysis of ellipsometric data which emphasizes the importance of line shape analysis.

Table III summarizes the variation of spin-orbit splitting in comparison with available data. Although the splitting is obtained from the separation of corresponding features in electroreflectance spectra, the literature data scatter considerably, a likely consequence of the large linewidth of room-temperature spectra. We find no significant difference of the bowing of Δ_0 and Δ_1, in striking contrast to results quoted for ternary alloys like In(As,P) and In(As,Sb) (Ref. 31) or (In,Ga)P (Ref. 32). Data of the spin-orbit splitting Δ_0' of the conduction band are scarce. Our value is much smaller than predicted from band structure calculations and varies far less with composition than the valence band splitting Δ_0 and Δ_1.

B. Influence of disorder

We discuss the influence of disorder as deviation from the virtual crystal approximation (VCA). This model assumes a periodic potential as the average of the potential in corresponding binary compounds and predicts a linear variation of energy gaps except for some deviation due to a changing lattice constant. The pioneering work of Van Vechten and Bergstresser (VVB) for ternary alloys showed that this intrinsic bowing is small and that bowing of energy gaps must be attributed to the aperiodic potential of randomly distributed ions on their sublattice.[1] They constructed the aperiodic disorder potential $V(y)$ from the different electronegativity C_{ion} of ions as derived from the dielectric theory of ionicity.[33] This theory models the dielectric constant of semiconductors by optical matrix elements between bonding and antibonding states and their mean energy gap which increases with respect to an equivalent covalently bound semiconductor due to ionic contributions to the strength of chemical bonds. The

TABLE II. Parameter and variance of a least-squares fit to a quadratic compositional shift of the energy gaps. Also listed are bowing parameters from the literature.

Gap	A (eV)	B (eV)	C (eV)
E_0	1.4187 (51)	−0.798 (21)	0.176 (19) 0.149,[a] 0.05,[b] 0.25,[c] 0.13,[d] 0.038[e]
$E_0+\Delta_0$	1.5278 (51)	−0.441 (20)	0.081 (25) 0.11[d]
E_1	3.2673 (78)	−0.974 (30)	0.381 (27) 0.222,[c] 0.21,[d] 0.184,[e] 0.33(5)[f]
$E_1+\Delta_1$	3.3917 (66)	−0.720 (27)	0.267 (23) 0.13,[d] 0.26 (4)[f]
E_0'	4.7314 (56)	−0.453 (25)	0.094 (24)
$E_0'+\Delta_0'$	4.8067 (56)	−0.368 (23)	0.059 (21)
$\delta(M_1)$	4.8786 (175)	−0.316 (71)	0.120 (66)
$\delta(M_0)$	4.9889 (87)	−0.224 (35)	0.048 (33)
E_2	5.1983 (168)	−0.459 (76)	0.155 (30)

[a]Reference 2.
[b]Reference 3.
[c]Reference 4.
[d]Reference 5.
[e]Reference 6.
[f]Reference 9.

TABLE III. Parameter and variance of least-squares fits to a quadratic variation of spin-orbit splitting in comparison to results from the literature.

Gap	A (meV)	B (meV)	C (meV)	
Δ_0	109 (3)	347 (10)	−101 (10)	This work
	119	300	−107	Ref. 4
	114	260	−20	Ref. 5
	123	173	54	Ref. 6
Δ_1	124 (5)	254 (20)	−114 (17)	This work
	145	173	−64	Ref. 4
	135	330	−20	Ref. 5
	146	183	−67	Ref. 6
	133	194	−70	Ref. 9
Δ_0'	75 (5)	85 (17)	−35 (16)	This work

model seemed particular suitable to model chemical trends. The disorder potential $V(y)$ mixes the Bloch states by intra- and interband scattering which causes the deviation $D(y)$ from the VCA gap [Eq. (1)]. We expect that this scattering is also responsible for alloy broadening of the van Hove singularities. The VVB model for ternary alloys has been extended to the lattice-matched pseudobinary compound (In,Ga)(As,P) assuming independent statistics on the cation and anion sublattices:[2]

$$D(x,y)=\frac{C_{\mathrm{III}}^2}{A}(1-x)x+\frac{C_{\mathrm{V}}^2}{A}(1-y)y. \tag{8}$$

C_j^2 is the square of the electronegativity difference of the ions on each sublattice and A is a bandwidth parameter. From the comparison of a large number of ternary alloys VVB proposed a universal value $A=1$ eV. Lattice matching ($y=2.14x$) leaves only one free compositional parameter and reduces Eq. (8):

$$D(y)=y\,\frac{0.467C_{\mathrm{III}}^2+C_{\mathrm{V}}^2}{A}-y^2\frac{0.218C_{\mathrm{III}}^2-C_{\mathrm{V}}^2}{A}$$

$$=[0.226y-0.152y^2]\ \text{eV}. \tag{9}$$

The last expression uses $C_{\mathrm{III}}^2/A=0.297$ eV and $C_{\mathrm{V}}^2/A=0.087$ eV, which are average values of the electronegativity difference in corresponding ternary compounds.[1] The quadratic term is the experimental bowing parameter C in Eq. (1). VVB predict that the very local character of the disorder eliminates a strong k dependence of the scattering terms and concluded that gaps between a pair of valence and conduction band show the same bowing, independent of the position in the Brillouin zone. This prediction applies to the gaps E_0, E_1, and E_2, which all should show the universal bowing according to Eq. (9) in obvious disagreement with the data.

While in ternary alloys $D(y)$ describes the deviation of the gap from the linear interpolation between the gap of the binary compounds $\mathcal{A}$ ($y=0$) and $\mathcal{B}$ ($y=1$) and is identical to the experimental bowing parameters C, this is not true for the quaternary alloys since the compound $\mathcal{B}$, $In_{0.53}Ga_{0.47}As$, is a ternary alloy with large disorder on the cation sites. Linear and quadratic terms of the bowing potential $D(x,y)$ have been evaluated from the compositional shift of the gaps and the difference of the gaps of InP and the VCA gap of $In_{0.53}Ga_{0.47}As$. The results are listed in Table IV and the corresponding bowing potentials are shown in Fig. 12. The dashed curve represents the universal bowing of the VVB model according to Eq. (9), which reproduces the common trend of bowing due to the random distribution of ions. The actual bowing of the gaps remains very different and is particularly large for E_1, which shows large alloy broadening.

The failure of universal bowing can be understood by a closer look at the terms C_j^2/A. In second-order perturbation theory VVB's bowing potential is an average $\langle|V_{nk,n'k'}|^2/(\Delta E_{nk,n'k'})\rangle$ of scattering matrix elements $V_{nk,n'k'}$ between band states which are separated by $\Delta E_{nk,n'k'}$. Interband scattering ($n=c$ and $n'=v$) will increase the gap, while intraband scattering pushes both the top valence band and the lowest conduction band into the gap region. The sign of bowing reveals the dominance of intraband scattering. By accounting in a simple model for the distribution of states, but keeping the common matrix element, Stroud confirmed the downshift of the smallest band gap and found decreasing bowing for higher-lying gaps[7] in agreement with the small bowing $D(x,y)$ of the high-lying gaps E_0' and E_2. This small bowing of these gaps must be anticipated since the sign of $\Delta E_{nk,n'k'}$. determines the direction of the direction of the shift of a state $|n,k\rangle$ by coupling to

TABLE IV. Energy gaps and spin-orbit splitting of InP ($y=0$) and of $In_{0.53}Ga_{0.47}As$ ($y=1$) in the virtual crystal approximation. $D(x,y)=\xi(1-x)x+\eta(1-y)y=a_1y+a_2y^2$ describes the reduction of the gap with respect to the VCA values for lattice-matched samples ($y=2.14x$) and the effective disorder potentials ξ and η of the cation and anion sublattice, respectively.

Gap	InP	$In_{0.53}Ga_{0.47}As$	a_1 (meV)	a_2 (meV)	ξ (meV)	η (meV)
E_0 (eV)	1.418	0.933	305	−176	518	63
E_1 (eV)	3.267	2.813	520	−381	558	259
E_0' (eV)	4.731	4.436	158	−94	257	38
E_2 (eV)	5.198	4.926	187	−155	128	127
VVB			226	−152	297	87
Δ_0 (meV)	109	357	−99	101	−8	−103
Δ_1 (meV)	124	245	−124	114	−40	−105

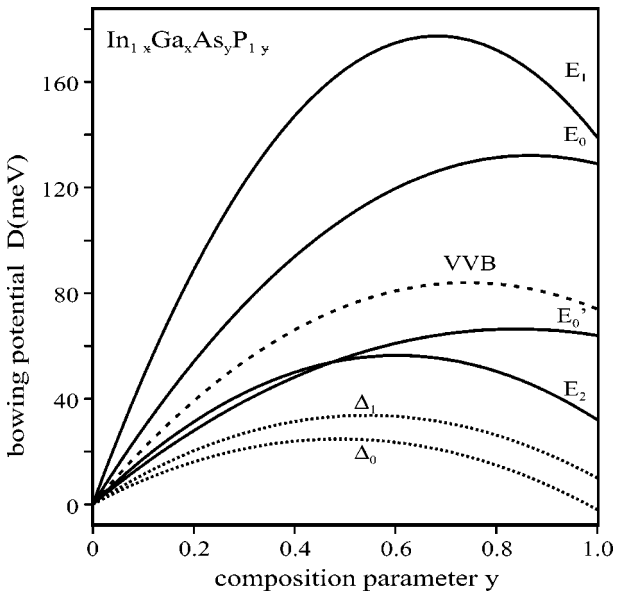

FIG. 12. Deviation $D(x,y)$ of gap energy and spin-orbit splitting of lattice-matched samples from the value predicted by the virtual crystal approximation. The dashed line shows the universal curve predicted from the VVB model (Ref. 2).

$|n',k'\rangle$. In a high density of states region like the conduction bands at E_0' and E_2 interactions with states at higher and lower energy begin to cancel, an effect which is absent at the bottom of the conduction band.

The significantly larger bowing of E_1 compared to the gap E_0 between the same bands could result from interband scattering. The large optical dipole moment between the *p*-type valence and *s*-type conduction band suggests some coupling of these bands by the disorder potential which has dipolar components. Since E_0 is 2 eV smaller than E_1, this repulsive coupling should be most effective for E_0 and reduces the bowing due to intraband scattering. We discard this explanation since it is not consistent with the large contribution of E_1 to the dielectric constant while the contribution of E_0 is negligible. Dipolar coupling of valence and conduction bands should rather reduce the bowing of E_1. We attribute the larger bowing of E_1 to intraband scattering in the conduction band. The lowest conduction band at *L* is closer to the high density of conduction band states along the Δ and Σ axes than the band minimum at Γ. If the scattering matrix elements are not much different, interband scattering is larger at *L*, which is consistent with the significantly larger broadening of the spectra at E_1. A similar difference of intraband scattering is expected for the top valence band at *L* and Γ. Details of the band structure thus are important for the bowing of gaps and for alloy broadening. Indeed, band structure calculations for ternary alloys find increasing broadening of van Hove singularities going from Ga(As,P), to (Ga,In)As and (Ga,In)P.[34]

For the ternary alloy disorder exists only on the cation sublattice and is near its maximum for $x=0.5$. The large bowing potential of E_1 and E_0 for the ternary alloys and the large spectral linewidth of the ternary compound are a consequence of the large compositional fluctuation on the cation site and are consistent with a larger difference of the electronegativity of Ga and In in the VVB model. The disorder potential in Eq. (8) has contributions from fluctuations on each sublattice which contribute to bowing according to scattering matrix elements and density of states. By analogy to the VVB model effective bowing potentials $\xi=\langle C_{\mathrm{III}}^2/A\rangle$ and $\langle \eta=C_{\mathrm{V}}^2/A\rangle$ have been derived from the linear and quadratic terms of the bowing potential $D(x,y)$ for each gap which are listed in Table IV. The values confirm that bowing of the gaps E_0 and E_0' at Γ is most sensitive to disorder on the cation sublattice. The off-center gaps, however, show considerable scattering potential η of fluctuations on the anion sites which are above its strength predicted from the VVB model. The effective bowing potentials indicate that van Hove singularities responds differently to disorder on the ion and cation sublattices which suggests that not only the distribution of states but also the scattering matrix element varies.

The spin-orbit splitting of the valence band at Γ and *L* is larger than their VCA value which points to coupling of the $j=3/2$ and $j=1/2$ valence bands by the disorder potential. We do not observe a different sign of bowing of Δ_0 and Δ_1, which has been reported in some ternary alloys of small gaps like In(As,Sb) and (In,Ga)As.[31] Reversed bowing of Δ_0 in these compounds has been attributed to admixture of *s*-like conduction band states by disorder, i.e., interband scattering, which increases as the gap get smaller.[35] Increasing *s* character of the *p*-type valence band reduces spin-orbit coupling and may play a role in small gap semiconductors. The present data show that for (InGa)(AsP) such a coupling is negligible since both Δ_0 and Δ_1 have very similar bowing and the remaining difference is probably not significant in view of the variance of the data. $D(x,y)$ of the valence band splitting reaches its maximum near $y\approx 0.5$ where the disorder on the anion sublattice is largest and vanishes for the ternary compound $(y=1)$ in striking contrast to the bowing of the gaps. We find also that in contrast to the gaps the effective disorder potential of the anions is significantly larger than of the cations ($\eta>\xi$). This result indicates that spin-orbit splitting of the valence band is sensitive only to disorder on the anion sublattice.

V. CONCLUSION

Electroreflectance spectroscopy at low temperature provides the sensitivity and spectral resolution which are needed to derive the compositional variation of energy gaps with sufficient precision. Line shape analysis which treats lifetime and field broadening of band states simultaneously improves the accuracy of the energy of van Hove singularities and identified the sequence of bands in a multiplet of transitions near 5 eV. Electroreflectance spectra at the fundamental gap are already at small fields in the high-field regime and fields contribute also to the spectral width line shape at higher gaps despite increased lifetime broadening.

The nonlinear shift of the energy gaps varies significantly for different gaps. Particular large bowing is found for the gap E_1 at *L*. The deviation $D(x,y)$ of the compositional shift from the virtual crystal approximation is attributed to scattering by the aperiodic disorder potential. The data are con-

sistent with a disorder potential which arises from different electronegativities of the ions on the respective sublattice. Disorder reduces the gaps which in second-order perturbation theory corresponds to dominant intraband scattering. Intraband scattering can also account for the smaller bowing of high-lying energy gaps.

The deviation of gaps at Γ from the virtual crystal approximation reaches its maximum at compositions where compositional fluctuation on the cation site is substantially larger as on the anion sublattice. This is consistent with the larger electronegativity difference of the cations. Effective disorder potentials are derived which distinguish scattering by anion and cation fluctuations for each gap. Gaps at the zone center are most sensitive to disorder on the cation sites which explains also the large linewidth observed in ternary alloys. For the noncenter gaps E_1 and E_2 scattering on the anion sites becomes stronger than predicted by the difference of electronegativities. These differences indicates that scattering matrix elements vary significantly for different gaps.

Disorder increases the spin-orbit splitting of the valence band in Γ and L which is attributed to disorder-induced coupling of the $j=3/2$ and $j=1/2$ subbands without significant difference of the bowing of Δ_0 and Δ_1. The bowing reaches the maximum at $y \approx 0.5$, i.e., for maximum fluctuation on the anion site, and vanishes for the ternary compound: This compositional variation differs from bowing of the gaps and indicates that spin-orbit splitting of the valence band is not sensitive to disorder on the cation sublattice.

The significantly different bowing and alloy broadening of the various singularities of the band structure can be understood by intraband scattering on the disorder potential, but predictions need more detailed consideration of the relevant matrix elements and energy separations to achieve meaningful average values.

ACKNOWLEDGMENTS

C.R. thanks the Deutsche Forschungsgemeinschaft for support. We appreciate the cooperation with Alcatel-SEL in several projects which supplied the samples used in this study.

[1] J. A. Van Vechten and T. K. Bergstresser, Phys. Rev. B **1**, 3351 (1970).
[2] T. P. Pearsall and C. Hermann, in *Proceedings of the International Symposium on GaAs and Related Compounds*, Japan, 1981, Inst. Phys. Conf. Ser. No. 63 (Institute of Physics, Bristol, 1982), p. 269; T. P. Pearsall, in *GaInAsP Alloy Semiconductors*, edited by T. P. Pearsall (Wiley, Chichester, 1982), Chap. 12.
[3] K. Nakayama, A. Yamaguchi, K. Akita, and T. Kotani, J. Appl. Phys. **49**, 5944 (1978).
[4] E. H. Perea, E. E. Mendez, and C. G. Fonstad, Appl. Phys. Lett. **36**, 978 (1980).
[5] P. M. Laufer, F. H. Pollak, R. E. Nahory, and M. A. Pollack, Solid State Commun. **36**, 419 (1980).
[6] J. A. Lahtinen and T. Tuomi, Phys. Status Solidi B **130**, 637 (1985).
[7] D. Stroud, Phys. Rev. B **5**, 3366 (1972).
[8] D. E. Aspnes and J. E. Rowe, Phys. Rev. Lett. **27**, 188 (1971).
[9] S. M. Kelso, D. E. Aspnes, M. A. Pollack, and R. E. Nahory, Phys. Rev. B **26**, 6669 (1982).
[10] D. E. Aspnes and J. E. Rowe, Solid State Commun. **8**, 1145 (1970).
[11] D. E. Aspnes, Phys. Rev. **153**, 972 (1967).
[12] D. E. Aspnes, in *Semiconductors and Semimetals*, edited by R. K. Willardson and A. C. Beer (Academic, New York, 1972), Vol. 9, p. 457.
[13] D. E. Aspnes, Phys. Rev. Lett. **28**, 168 (1972).
[14] A. Jaeger, G. Weiser, P. Wiedemann, I. Gyuro, and E. Zielinski, J. Phys.: Condens. Matter **8**, 6779 (1996).
[15] A. Jaeger and G. Weiser, Phys. Rev. B **58**, 10 674 (1998).
[16] A. Jaeger, G. Weiser, and P. Wiedemann, IEEE J. Sel. Top. Quantum Electron. **1**, 1113 (1995).
[17] M. Cardona, K. L. Shaklee, and F. H. Pollak, Phys. Rev. **154**, 696 (1967).
[18] B. O. Seraphin and N. Bottka, Phys. Rev. **145**, 628 (1966).
[19] F. H. Pollak, W. Krystek, M. Leibovitch, M. L. Gray, and W. S. Hobson, IEEE J. Sel. Top. Quantum Electron. **1**, 1002 (1995).
[20] N. H. Lu and T. M. Hsu, Phys. Rev. B **52**, 8191 (1995).
[21] W.-H. Chang, T. M. Hsu, W. C. Lee, and R. S. Chuang, J. Appl. Phys. **83**, 7873 (1998).
[22] H. I. Ralph, J. Phys. C **1**, 378 (1968).
[23] D. F. Blossey, Phys. Rev. B **2**, 3976 (1970).
[24] D. E. Aspnes and A. A. Studna, Phys. Rev. B **7**, 4605 (1973).
[25] D. S. Kyser and V. Rehn, Solid State Commun. **8**, 1437 (1970).
[26] J. R. Chelikovsky and M. L. Cohen, Phys. Rev. B **14**, 556 (1976).
[27] D. E. Aspnes, Phys. Rev. Lett. **31**, 230 (1973).
[28] H. J. Kolbe, C. Agert, W. Stolz, and G. Weiser, Phys. Rev. B **59**, 14 896 (1999).
[29] D. E. Aspnes, J. Opt. Soc. Am. **63**, 1380 (1973).
[30] R. J. Elliott, Phys. Rev. **108**, 1384 (1957).
[31] S. S. Vishnubhatla, B. Eyglunent, and J. C. Woolley, Can. J. Phys. **47**, 1661 (1969).
[32] C. Alibert, G. Bordure, A. Laugier, and J. Chevalier, Phys. Rev. B **6**, 1301 (1972).
[33] J. C. Phillips, Phys. Rev. Lett. **20**, 550 (1968).
[34] Y.-T. Shen and C. W. Myles, J. Phys. Chem. Solids **48**, 1173 (1987).
[35] O. Berolo, J. C. Woolley, and J. A. Van Vechten, Phys. Rev. B **8**, 3794 (1973).